ingegneria sismica
International Journal of Earthquake Engineering
Anno XLIII - Num. 2 - 2026

Research on state estimation method and application of multi-source data fusion in smart distribution network

Zhen Jin[1] *and Yibo Zhou*[1,*]

[1] Northeast Electric Power University, Jilin City, Jilin Province, 132000, China

SUMMARY: *Traditional smart distribution network state estimation faces some problems, such as out-of-sync sampling, missing measurements, topology changes, and heterogeneous data formats of SCADA, PMU, smart meters, feeder terminals and environmental sensors. This paper proposes a state estimation model for multi-source data fusion, which unifies asynchronous measurements in the framework of graph-aware computing. Buses, feeders, and transformers are represented as topological embeddings, and irregular measurements are aligned through a time-fused encoder weighted by sources-level confidence. The layer output node voltage, phase Angle, branch current, active and reactive power states are estimated, and the calibration component identifies abnormal measurements and accounts for confidence changes. The model is tested on the IEEE 33-node distribution network simulation dataset, which contains 52,800 samples, and the provincial distribution network dataset, which contains 286,000 operating records. Experimental results show that in the actual online deployment scenario, the proposed model reduces the voltage MAE to 0.0136 p.u., the state recognition accuracy reaches 96.2%, and the average inference delay is 18.7 ms.*

KEYWORDS: *Multi-source data fusion; State estimation; Graph neural network; Smart distribution network*

1 Introduction

The smart distribution network undertakes the tasks of distributed power access, bidirectional power flow regulation, load-side response and equipment status perception. The operation data has changed from a single measurement to a multi-terminal, multi-frequency and multi-scale form. SCADA, PMU, smart meters, feeder terminals, station area sensors and meteorological load records enter the system, and state variables such as node voltage, phase Angle, branch current, active power and reactive power show time series fluctuation and topology coupling. As the computational basis of online sensing in distribution network, state estimation needs to generate stable results under the conditions of missing measurements, noise disturbance, inconsistent sampling interval and topology switching. It is difficult to adapt to the data environment after distributed energy and massive terminal access by relying only on traditional weighted least squares or static pseudo-measurements.

Around distribution network state estimation, Rout et al. proposed a dynamic matrix completion method to recover missing measurements and correct node states [1]. Raghuvamsi et al. proposed a deep learning detection and reconstruction framework for measurement corruption under false data injection and denial of service attacks, so that abnormal measurements can be identified and repaired before estimation [2]. Asefi et al. combined

*zhouyibocc@126.com
https://doi.org/10.65102/is2026924
Published: 30 April, 2026

model-driven method and data-driven method for anomaly detection and classification in power system state estimation [3]. Ganjkhani et al. studied the application of machine learning in the location and resolution of state estimation anomalies, indicating that the data model can assist in the identification of measurement deviations and operating state changes [4]. These researches extend the state estimation from pure numerical solution to data quality identification, exception recovery and intelligent correction, but the time alignment, confidence assignment and topological dependence expression between multi-source data still need a unified computing framework.

With the development of graph learning and deep neural networks, distribution network state estimation has shifted from measurement equation solving to structured feature learning. Kundacina et al. proposed a linear state estimation method of graph neural network based on factor graph, which enhanced the robustness and scalability under PMU measurement conditions [5]. Habib et al. proposed a deep statistical solver to combine the idea of statistical estimation with the deep model for the state variable prediction of distribution system [6]. Dabush et al. used graph signal processing tools to study partially observable power system state estimation, so that topology structure and observation sparsity could be jointly involved in the calculation [7]. Cooper et al. sorted out the research direction of state estimation from the perspective of anomaly detection, emphasizing the correlation between operational data security and estimation credibility [8]. Vijaychandra et al. summarized the distribution system state estimation methods and their application scenarios, and pointed out that measurement sparsity and pseudo-measurement dependence in low-voltage distribution network still affected the estimation accuracy [9]. Bekesi et al. proposed a state estimation method of distribution system based on deep neural network and hyperparameter optimization to improve model adaptation ability under parameter combination [10].

Based on the above research basis, this paper constructs a multi-source data fusion state estimation model for smart distribution grid. The model takes multi-source operational data as input, and forms a unified representation through timestamp alignment, missing compensation and measurement confidence assignment. At the topological level, the bus, feeder, transformer, switch state and branch connection relationships are embedded into the graph structure space to realize the joint mapping between the physical network and the measurement space. At the estimation level, the graph neural network is used to extract the node correlation features, and the timing coding module is combined to describe the dynamic response under load fluctuation, distributed power output variation and environmental disturbance. The model outputs the node voltage, phase Angle, branch current and power state. At the same time, the reliability check and interpretable analysis are introduced to track the source of abnormal measurement, the distribution of estimation deviation and the key state variables. The following chapters will expand from literature review, model construction, experimental evaluation and discussion to verify the applicability of the fusion computing framework in state estimation accuracy, state discrimination and online applications, as well as edge deployment.

2 Literature Review

2.1 Traditional calculation methods for distribution network state estimation

The traditional calculation methods of distribution network state estimation mainly rely on measurement equations, topological parameters and electrical constraints to solve the node state. The core of the method is to infer the voltage, phase Angle and branch power that

cannot be directly observed according to a limited number of measurements. The distribution of measurement points in low-voltage distribution network is uneven, and the power flow direction and voltage distribution are more prone to local changes after the access of distributed power sources and adjustable loads. The traditional calculation process usually relies on spurious measurements, weighted least squares, power flow correction and equipment control parameters to maintain the stability of estimation.

Taczi et al. studied the role of voltage control equipment in the process of low-voltage state estimation, and pointed out that voltage regulators, tap switches and reactive power compensation devices will change the node voltage boundary, and the estimation results are easy to deviate from the actual operation state if the equipment action information is ignored in state estimation [11]. Barancsuk and Hartmann analyzed the influence of pseudo-measurement selection and real measurement access on the accuracy of distribution network state estimation, indicating that the quality of pseudo-measurement, the degree of measurement redundancy and the location of real sampling points will directly affect the stability of traditional estimation results [12]. These methods have the characteristics of clear physical meaning, interpretable calculation process and low engineering implementation threshold, which are suitable for distribution network scenarios with stable topology and limited number of measurements. However, they need to rely on strong prior assumptions when multi-source data is accessed asynchronously and node status changes rapidly.

Nguyen et al. proposed space-time cyclic graph neural network for fault diagnosis of distribution system. Related studies show from the side that it is difficult to cover the spatial propagation and time evolution characteristics of operation state only by static measurement equation [13]. Alhanaf et al. studied a smart grid fault detection and classification scheme based on deep neural networks, and showed that the data-driven model can extract more complex state patterns from voltage, current and power waveforms [14]. Tabassum et al. proposed an inverter microgrid network physical anomaly detection method based on autoencoder neural network, and the results reflect that the traditional estimation chain still has limited ability to identify hidden states in the face of the coexistence of power electronic equipment, communication disturbances and abnormal measurements [15].

From the perspective of computer implementation, traditional state estimation usually uses measurement matrix, Jacobian matrix and weight matrix as the main calculation objects, and the iterative solution process relies on measurement residual and convergence threshold to complete state correction. The flow is easy to be embedded in the dispatching automation system, and easy to connect with the database, topology analysis module and power flow calculation program. In the actual deployment, the SCADA sampling period is long, the smart meter data upload delay, and the measurement accuracy of the feeder terminal is not completely consistent. The traditional method needs to complete the screening, completion and weight setting before the data enter the estimator. If the measurement source changes, the weight matrix often needs to be readjust, and the model parameters are difficult to update adaptively with the running state. At the same time, most of the traditional estimators use the central server as the calculation carrier, which is difficult to form a continuous processing link with the data caching, online anomaly screening and low-latency update of the edge terminal. Therefore, traditional calculation methods provide a solid physical constraint foundation for distribution network state estimation, but their adaptability to missing data, noisy measurements, dynamic topology and multi-source heterogeneous inputs is insufficient, and it is difficult to directly undertake complex information fusion tasks in online estimation of smart distribution network.

2.2 Multi-source data fusion and machine learning state estimation method

The research focus of multi-source data fusion and machine learning state estimation methods has gradually shifted from single measurement supplement to unified representation of data space and intelligent inference of state variables. The data in smart distribution grid is not only from the primary device measurements, but also includes communication links, edge terminals, user-side sampling, distributed power output and meteorological load characteristics. Different data sources have differences in sampling period, accuracy level, missing form and security risk. The state estimation model needs to complete time alignment, feature coding, confidence weight allocation and abnormal input screening at the computational level. Mirzaee et al. studied the transformation of smart grid security and privacy from traditional mechanisms to machine learning mechanisms, and pointed out that machine learning can be used to identify risks of data injection, communication attacks and privacy leakage, which provides a computational basis for security measurement screening in state estimation [16]. Biswal et al. summarized the application of machine learning and deep learning in load forecasting of smart grid, and showed that historical load, meteorological variables and user behavior data can form auxiliary state features to provide data support for pseudo-measurement estimation in low observation areas [17]. As shown in Table 1, related research has entered the distribution network state estimation link from the directions of load forecasting, safety detection, pseudo measurement generation and critical state identification, forming the basic path of multi-source fusion calculation.

Table 1: Comparison of related studies on multi-source data fusion and machine learning state estimation

Research Direction	Main Data Sources	Computational Method	Implications for State Estimation
Smart grid security perception	Communication logs, operation alarms, measurement records	Machine learning-based threat identification	Supports the identification of abnormal measurement sources
Load forecasting and state assistance	Historical load, meteorological data, user-side data	Machine learning and deep learning prediction	Provides dynamic support for pseudo-measurement generation
Information fusion estimation	SCADA, PMU, pseudo-measurements	Bayesian inference	Supports credibility modeling of multi-source measurements
Pseudo-measurement generation	User load, historical power, topology information	Generative neural networks	Alleviates data insufficiency in low-observability areas
Attack detection and state estimation	Node voltage, power, communication disturbance	Multi-output deep neural network	Supports collaborative estimation and security detection
Critical state identification	Behavior-related data, measurement sequences	Behavioral correlation analysis	Supports operation state identification and early warning

Massignan et al. proposed an information fusion Bayesian inference method for distribution system state estimation, which converts measurements from different sources into probability expressions, so that measurement credibility can enter the estimation process [18]. Da Silva et al. proposed a generative neural network method for pseudo-measurement generation in distribution systems, which mapped historical load and operation data into inputs that could be used for estimators to improve state observability in sparse measurement areas [19]. Radhoush et al. proposed a multi-output deep neural network, which combined

distribution system state estimation with false data injection attack detection, and the model could simultaneously output node state and attack recognition results [20]. Buchta et al. studied the behavior correlation in distribution system state estimation, and used the correlation between operation modes to identify the critical system states, so that the state estimation results could serve the operation state discrimination [21].

These studies show that the value of machine learning methods lies not only in fitting state variables, but in transforming multi-source data into computable, verifiable, and traceable state representations. Compared with the traditional estimation, the deep model can extract nonlinear relationships from high-dimensional inputs, the graph structure model can express the topological dependence between nodes, branches and switch states, the generative model can compensate for the lack of measurements, and the security detection model can filter the untrusted input. From the perspective of system implementation, multi-source fusion state estimation also needs to deal with the calculation details such as inconsistent database fields, timestamp drift, edge terminal cache delay and dynamic change of measurement confidence.

The slow SCADA measurement can be used as the reference state, the high-frequency data of PMU and feeder terminal can be used as the local correction information, and then the smart meter and load prediction results are converted into pseudo-measurement input to form a hierarchical fusion structure. This structure is convenient to distinguish real-time measurements, historical inference and model completion data in online estimation, and reduce the influence of single source anomaly on global estimation. In the model training phase, sample slices, normalized scales and topological versions should also be recorded synchronously to ensure that the estimation results are double-checked. The state estimation for smart distribution grid still needs to put multi-source fusion, topology representation, credibility verification and interpretable output into the same computing framework, so that the estimation results can not only maintain numerical accuracy, but also correspond to specific scenarios such as voltage overruns, load anomalies and branch operation risks.

3 State estimation model of multi-source data fusion in smart distribution network

3.1 Multi-source operation data fusion and state feature construction

The inputs for smart distribution grid state estimation come from SCADA, PMUs, smart meters, feeder terminals, environmental sensors, and load forecasting records. The sampling period, field granularity and communication delay of different terminals are not consistent. If the node state is directly concatenated into a unified matrix, time offset and source confusion will occur. In this section, multi-source operation data are organized into state characteristics oriented to estimation tasks, so that measurements, source labels, time Windows and confidence can be simultaneously retained at each estimation moment.

The state feature construction takes the node as the basic object, and forms data slices around voltage amplitude, phase Angle proxy, branch current, active power, reactive power, load change rate, environmental disturbance and equipment operation mark. Before slices enter the model, time alignment, credibility assignment, missing compensation and feature projection need to be completed to avoid low-frequency data covering high-frequency fluctuations and to avoid abnormal upload values being amplified in the fusion stage.

In order to push measurements with different sampling frequencies into a unified estimation window, a time alignment kernel with source weights is constructed, which is calculated as follows:

$$\tilde{x}_{s,i,t}^{(m)} = \frac{\sum_{\tau \in \Omega_t} \exp\left(-|t-\tau|/\lambda_s\right) x_{s,i,\tau}^{(m)}}{\sum_{\tau \in \Omega_t} \exp\left(-|t-\tau|/\lambda_s\right)} \tag{1}$$

Here,$\tilde{x}_{s,i,t}^{(m)}$ represents the m alignment measurement obtained by data source s at node i and time t. Let Ω_t denote the time window around the current estimated time; Letλ_s denote the source-level time attenuation coefficient. The formula assigns weights according to the time distance, so that the PMU high-frequency segment, the SCADA slow measurement and the smart meter cycle data form a consistent expression in the same estimation window.

In order to avoid low-quality measurements directly entering the fusion vector, it is necessary to calculate the confidence weight according to the communication quality, residual offset and missing state, which is calculated as follows:

$$c_{s,i,t} = \sigma(\alpha q_{s,i,t} - \beta r_{s,i,t} - \gamma \delta_{s,i,t} + \eta_s) \tag{2}$$

where $c_{s,i,t}$ and t represent the measurement confidence weight. $q_{s,i,t}$ denote the communication link quality; $r_{s,i,t}$ represent the deviation degree of measurement residual error; Let $\delta_{s,i,t}$ denote missing, delayed, or abnormal upload markers; α,β,γ,η_s are trainable parameters. This formula converts the data quality into continuous weight instead of simply deleting abnormal samples, which can retain the reference value of edge terminals in local states.

After the confidence calculation is completed, all kinds of measurements, external attributes and node static information are mapped into a unified feature space. The fusion process is shown in the following equation:

$$z_{i,t} = \mathrm{Concat}\left(\sum_{s=1}^{S} c_{s,i,t} W_s \tilde{x}_{s,i,t}, u_{i,t}, b_i\right) \tag{3}$$

where $z_{i,t}$ represent node fusion features; W_s represents the mapping matrix of different data sources. $\tilde{x}_{s,i,t}$ denote the aligned multidimensional measurements; $u_{i,t}$ denotes external attributes such as load, weather, and distributed power output; b_i represents node type, capacity level, and area attributes. This formula makes the measurement data and the operating background enter the state estimation model together.

For short-time missing, terminal offline and communication delay samples, the historical state and neighborhood state are jointly compensated, which is calculated as follows:

$$\bar{z}_{i,t} = \rho_{i,t} z_{i,t} + (1-\rho_{i,t})\left(W_h z_{i,t-1} + \frac{1}{|\mathcal{N}_i|}\sum_{j \in \mathcal{N}_i} W_n z_{j,t}\right) \tag{4}$$

where $\bar{z}_{i,t}$ represent the node features after compensation. Let $\rho_{i,t}$ denote the data completeness; $\mathcal{N}_i$ represents the set of neighboring nodes; W_h and W_n denote the historical state and neighborhood state mapping matrices, respectively. This formula uses temporal continuity and spatial proximity to repair the shortage samples, so that the terminal station area and low observation nodes can still form stable inputs.

Fig. 1 is used to present the processing path of the multi-source operational data before it enters the state estimation model. The left side of the figure corresponds to different data entries, including SCADA measurements, PMU snapshots, smart meter curves, feeder terminal data and environmental sensor records. The middle layer corresponds to the

computing processing layer, which completes time alignment, credibility calculation, missing compensation and fusion coding in turn. The right side corresponds to the model input results, the output node state feature tensor, the data quality label, and the estimated cache index. This figure emphasizes the correspondence between data sources, processing steps, and model entries, enabling subsequent state estimation to trace the origin of each input feature.

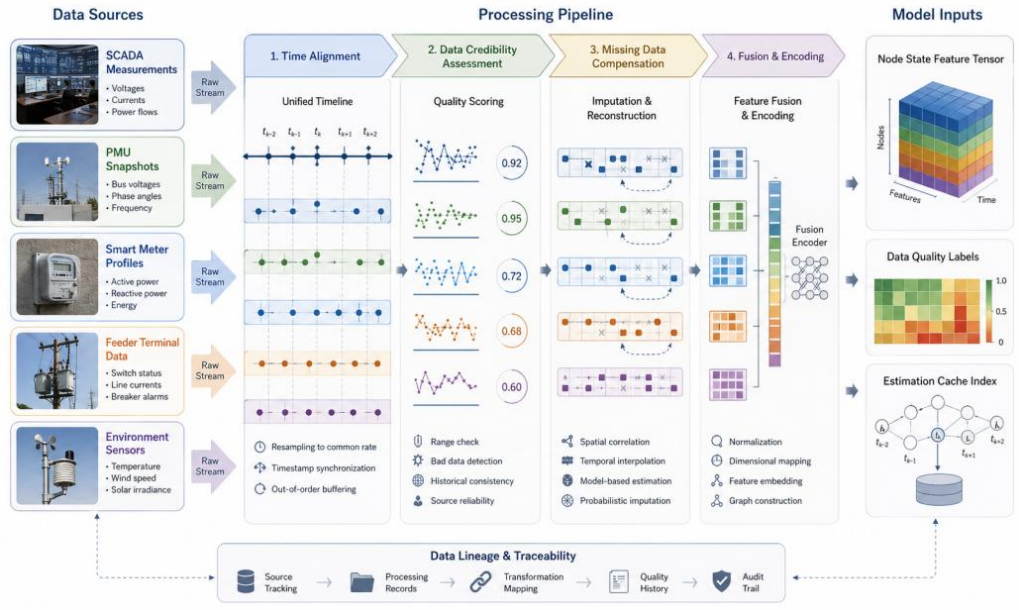

Figure 1: Multi-source operational data fusion and state feature construction process

In order to make the fusion result directly enter the subsequent topological embedding layer, it is necessary to generate the state input tensor of uniform dimension, which is expressed as follows:

$$H_t^0 = \mathrm{LayerNorm}\left(Z_t W_f + 1 b_f^\top\right), \quad Z_t = [\bar{z}_{1,t}, \bar{z}_{2,t}, \ldots, \bar{z}_{N,t}]^\top \tag{5}$$

Here, H_t^0 represents the initial input tensor of the state estimation model. Z represents the fusion feature matrix of all nodes. W_f and b_f denote the projection parameters; LayerNorm is used to stabilize the numerical scale of different nodes. This formula provides a uniform interface for subsequent topology embedding, and also enables sample slices, terminal sources and quality labels to be kept synchronously in the model link.

After the above processing, the multi-source data no longer enters the state estimator as an isolated field, but is transformed into computational features with temporal semantics, source confidence and node affiliation. This feature is suitable for both offline training and online inference. For feeders with obvious load fluctuation, the model can retain short-term variation. For terminals with low upload frequency, neighborhood compensation can maintain input continuity. For sensors with communication jitter, the trusted weight can reduce its disturbance to the estimation results.

3.2 Distribution network topological relationship embedding and measurement space mapping

After the multi-source state features are constructed, they also need to fall into the topology space of the distribution network. Smart distribution network is composed of buses, feeders, switches, transformers, distributed power sources and load nodes. The relationship between

nodes will change with the switch division, station transfer and feeder reconstruction. If we only deal with the node characteristics and ignore the connection structure, the state estimation result may be close to the true value in the single point value, but it cannot reflect the branch power flow, voltage sag and the linkage relationship between adjacent nodes.

The role of topological relation embedding is to transform physical connections, line parameters and operating states into learnable structural representations. The function of measurement space mapping is to locate different fields in SCADA, PMUs, smart meters, and feeder terminals to node, voltage, phase Angle, branch current, and power states. Together, the two form the structural entry of the state estimation model, so that the multi-source characteristics not only stay at the data level, but also can be consistent with the operation logic of the distribution network.

In order to write the line impedance, switching state and power flow changes into the branch representation, the dynamic branch embedding vector is constructed, which is calculated as follows:

$$e_{ij,t} = \phi_e\left(W_e[r_{ij}, x_{ij}, s_{ij,t}, P_{ij,t}, Q_{ij,t}, \Delta V_{ij,t}]^\top + b_e\right) \tag{6}$$

where $e_{ij,t}$ denotes the embedding vector of branch (i,j) at time t; r_{ij} and x_{ij} denote the line resistance and reactance; $s_{ij,t}$ denotes the switch connected state; $P_{ij,t}$, $Q_{ij,t}$ and $\Delta V_{ij,t}$ represent branch active power, reactive power and voltage difference, respectively. Let ϕ_e denote the nonlinear mapping function. This formula encodes the static network parameters and dynamic running states in a unified way, avoiding the topology representation staying at the simple adjacency matrix level.

After branch embedding is formed, it is necessary to calculate the influence strength of neighboring nodes on the current node to make the topology transfer have direction and weight, which is calculated as follows:

$$a_{ij,t} = \frac{\exp(v^\top \tanh(W_a[h_{i,t}; h_{j,t}; e_{ij,t}]))}{\sum_{k\in\mathcal{N}_i} \exp(v^\top \tanh(W_a[h_{i,t}; h_{k,t}; e_{ik,t}]))} \tag{7}$$

where $a_{ij,t}$ represents the topological influence weight of node j on node i. $h_{i,t}$ and $h_{j,t}$ denote node state features; v and W_a denote trainable attention parameters; Let $\mathcal{N}_i$ denote the set of neighborhoods of node i. This equation can distinguish the main feeder, contact branch and weak coupling branch, so that the state influence of adjacent nodes enters the model according to the operation structure.

The measurement space mapping needs to align the fields in the different data sources with the state variables and establish the probabilistic relationship between the measurements and the topological position, which is defined as follows:

$$m_{k,t} = \mathrm{Softmax}\left(W_m[y_{k,t}; p_{o(k),t}; p_{d(k),t}; e_{o(k)d(k),t}] + b_m\right) \tag{8}$$

where $m_{k,t}$ represents the probability vector mapping the k measurement to the state space. $y_{k,t}$ denotes the original measurement field; $o(k)$ and $d(k)$ denote the starting point and ending point of the measurement association. $p_{o(k),t}$ and $p_{d(k),t}$ denote the node topological position embedding. The formula integrates field semantics, topological position and branch relationship into the mapping process, which reduces the state mismatch caused by inconsistent naming of different systems.

In order to write the neighborhood structure information into the node representation, the topological weights and branch embeddings need to be aggregated, which is calculated as

follows:

$$p_{i,t} = \mathrm{GRU}\left(h_{i,t}, \sum_{j \in \mathcal{N}_i} a_{ij,t} W_p e_{ij,t} \odot h_{j,t}\right) \tag{9}$$

where $p_{i,t}$ denotes the node embedding with topological relations; GRU is used to retain the node's own state and receive neighborhood information. GRU for element-wise multiplication; W_p represents the structural projection matrix. The equation introduces the operation influence of adjacent branches and neighborhood nodes on the basis of the original characteristics of nodes, which is suitable for switch state change and feeder power transfer scenarios.

Fig. 2 is used to illustrate the computational relationship between topological embedding and measurement space mapping. The left side of the figure shows the physical objects of the distribution network, including nodes, feeders, switches, transformers and distributed power sources. The middle layer is the structure calculation layer, including branch parameter coding, topological influence weight, measurement field location and state space mapping. The right side is the state estimation entry, which forms the joint input of node voltage, phase Angle, branch current, active and reactive power. The diagram is able to show the mapped links between the physical network, data fields, and state variables.

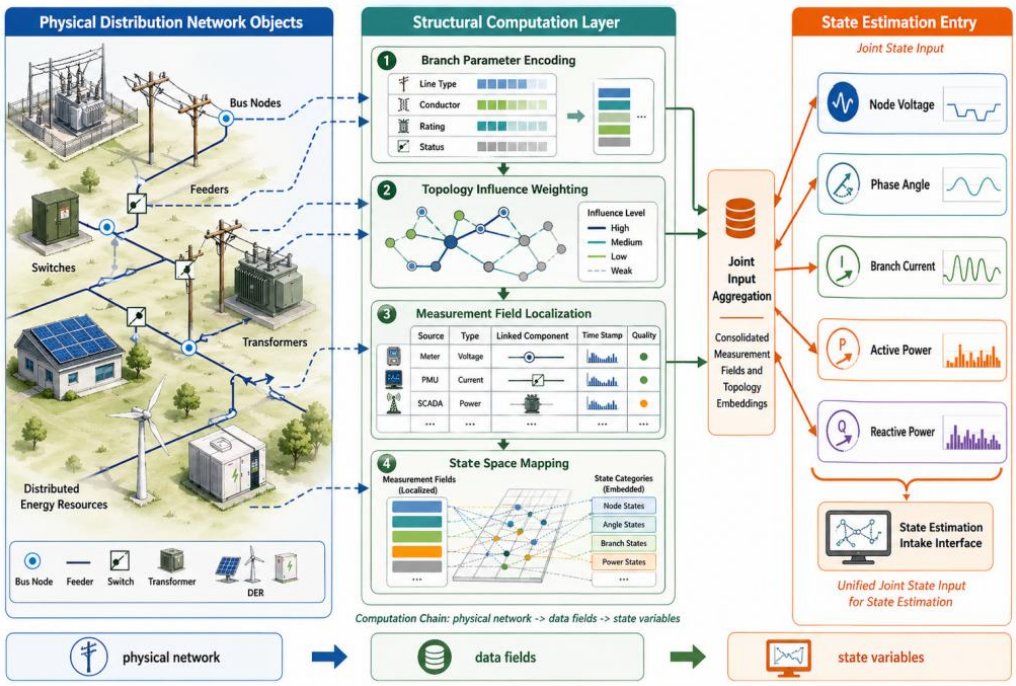

Figure 2: Distribution network topological relationship embedding and measurement space mapping process

After the topology aggregation and measurement bits are completed, the joint input matrix that the state estimation layer can call needs to be formed, which is calculated as follows:

$$R_t = \mathrm{Norm}\left(\sum_{k=1}^{K} m_{k,t}\, y_{k,t}^{\top}\right), \quad S_t^0 = \mathrm{Concat}(P_t, R_t) \tag{10}$$

Here, R_t represents the measurement space mapping matrix. K denotes the number of

available measurements at the current time; Norm stands for scale correction function. P_t represents the topological embedding matrix of all nodes. S_t^0 represents the joint topology-measurement input into the state estimation layer. This formula combines physical topology, measurement fields and state variables into a unified interface, so that the state estimation model can read structural constraints and observation evidence at the same time.

Through the above embedding and mapping, the distribution network topology is no longer just a static specification external to the model, but becomes part of the state estimation calculation. For feeders with frequent switching actions, branch embedding can reflect the connection changes in time. For low observation end nodes, neighborhood aggregation can provide structural complement. For the measurement system with complex fields, mapping probability can preserve the correspondence between fields and state variables. The processing provides a structured input for the subsequent state estimation results generation, running state discrimination and credibility verification, and also makes the estimation results have traceable physical location and data source.

3.3 Generation of state estimation results and discrimination of operating states

After feature fusion, topology embedding and measurement space mapping, the multi-source operation data has formed a joint input including node attributes, branch relationships and measurement evidence. The task of the state estimation layer is to transform this joint input into the state variables required for the operation of the distribution network and further form the discriminative operation state results. Unlike ordinary regression outputs, distribution network state estimation needs to simultaneously preserve numerical accuracy, topological consistency, and operational implications. There are obvious coupling relationships among node voltage, phase Angle proxy, branch current, active power and reactive power. If any variable is separated from the branch connection and the load change is output alone, the engineering usability of the estimation results will be weakened. Therefore, this section establishes a continuous computational link between state decoding, residual correction, branch reconstruction and operation state discrimination, so that the model output can be further transformed from numerical results to online monitoring callable state information.

In order to convert the joint topologic and measurement input into multi-dimensional state variables, a state decoder with the cooperation of shared encoding and task branch should be constructed, which is calculated as follows:

$$\hat{x}_{i,t} = [\hat{V}_{i,t}, \hat{\theta}_{i,t}, \hat{I}_{i,t}, \hat{P}_{i,t}, \hat{Q}_{i,t}] = \psi_o(S_t^0[i]W_o + b_o) \tag{11}$$

where $\hat{x}_{i,t}$ represents the state estimation vector of node i at time t, and $\hat{V}_{i,t}$, $\hat{\theta}_{i,t}$, $\hat{I}_{i,t}$, $\hat{P}_{i,t}$, $\hat{Q}_{i,t}$ represent the voltage amplitude, phase Angle proxy, branch current, active power and reactive power estimation respectively. $S_t^0[i]$ represents the joint topology-measurement input corresponding to the node. W_o and b_o denote the state decoding parameters; Let $\psi_o(\cdot)$ denote the nonlinear mapping function. This formula makes different state variables share the same underlying input, while retaining independent physical meaning at the output, which is convenient for subsequent itemization discrimination.

In actual operation, the local measurement may appear drift, delay or short-time abrupt change. In order to avoid the abnormal residual directly amplifying into the estimation results, the model sets a residual gated correction layer after state decoding, and only limited correction is performed on the high-confidence residual information.

In order to reduce the disturbance of local abnormal measurements on the state estimation

results, it is necessary to introduce the residual gated correction term and control the correction amplitude, which is calculated as follows:

$$x_{i,t}^{c} = \hat{x}_{i,t} + g_{i,t} \odot \tanh(W_r r_{i,t}), \quad g_{i,t} = \sigma(W_g[r_{i,t}; h_{i,t}] + b_g) \tag{12}$$

where $x_{i,t}^{c}$ represent the corrected state estimation results; $r_{i,t}$ denotes the residual error of node measurement; $g_{i,t}$ denotes the residual gating coefficient; W_r, W_g, and b_g denote trainable parameters; $\odot$ indicates element-wise multiplication. Instead of directly using the residual coverage estimate, this formula judges the correction intensity according to the residual and node characteristics, so that the influence of smart meter packet loss, feeder terminal drift and PMU local anomaly on the final result is constrained.

State estimation also needs to keep the structure between node states and branch states consistent. If the node voltages are reasonably estimated, but the branch currents do not match the power distribution, the results are still difficult to use for operation discrimination. Therefore, branch reconstruction calculation is added to the output layer.

In order to ensure that the node state and the branch state are consistent in the distribution topology, it is necessary to reconstruct the branch state according to the node voltage, phase Angle and line parameters, which is calculated as follows:

$$\ell_{ij,t} = s_{ij,t}\left[\frac{|\hat{V}_{i,t}e^{j\hat{\theta}_{i,t}} - \hat{V}_{j,t}e^{j\hat{\theta}_{j,t}}|}{\sqrt{r_{ij}^2 + x_{ij}^2} + \varepsilon},\ \hat{P}_{ij,t},\ \hat{Q}_{ij,t}\right] \tag{13}$$

Here, $\ell_{ij,t}$ denotes the reconstruction state of branch (i,j); $s_{ij,t}$ denotes the branch connectivity state; r_{ij} and x_{ij} denote the line resistance and reactance; Let ε denote the numerically stable term; $\hat{P}_{ij,t}$ and $\hat{Q}_{ij,t}$ denote the branch active and reactive power estimates. This equation connects the node estimation results with the branch operation relationship, so that the state output can reflect the conduction relationship between switching states, line parameters and voltage differences.

Fig. 3 is used to illustrate the generation and discrimination process of state estimation results. On the left side of the figure is the joint topology-measurement input formed in the previous section, including node features, branch embedding and measurement mapping matrix. The middle layer was the calculation layer, which completed multi-dimensional state decoding, residual gate correction and branch state reconstruction in turn. The right side is the running discrimination layer, which converts the continuous state variable into the running category. At the bottom is the application output, including the voltage limit indication, the load spike marker, the branch overload indication, and the recheckable result index.

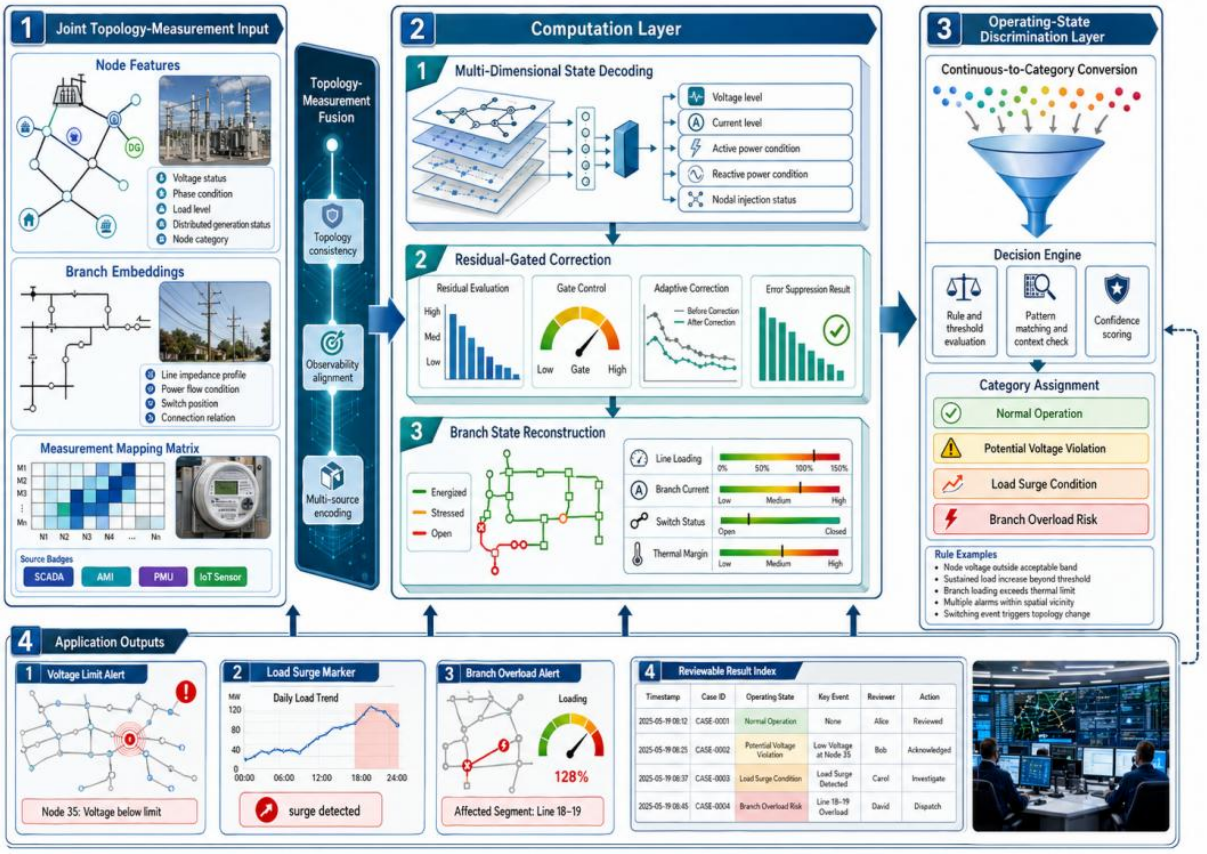

Figure 3: Process of state estimation result generation and running state discrimination

Continuous state variables need to be converted into running state labels before entering the monitoring platform and alarm module. The operating state discrimination not only depends on the single point threshold, but also integrates the state change rate, the neighborhood branch state and the load fluctuation amplitude.

In order to convert the continuous estimation results into operating state categories, a discriminant function integrating state changes and branch constraints should be constructed, which is calculated as follows:

$$p_{i,t}^{run} = \mathrm{Softmax}\left(W_c[x_{i,t}^c; \Delta x_{i,t}^c; \max_{j\in\mathcal{N}_i} \ell_{ij,t}] + b_c\right) \tag{14}$$

where $p_{i,t}^{run}$ represent the probability of the node or branch corresponding to each class of operating states. $\Delta x_{i,t}^c$ denote the state change at adjacent moments; W_c and b_c denote the discriminant layer parameters. This formula can distinguish voltage offset, load surge, branch overload and measurement anomaly states, so that the estimation results have clear operational meaning.

The running state discrimination results also need to be converted into response vectors that can be read by the system. The vector can be written into the result library, and can also be provided to the main station interface, edge terminal and operation and maintenance review module.

In order to make the state estimation results available for online operation, the discriminant probability, boundary offset and device label should be fused into a response vector, which is calculated as follows:

$$a_{i,t} = \sigma\left(W_a^r[p_{i,t}^{run}; v_{i,t}^{lim}; l_{i,t}^{rate}; d_{i,t}] + b_a^r\right) \tag{15}$$

where $a_{i,t}$ represents the running scenario response vector; $v_{i,t}^{lim}$ represent voltage boundary offset features; $l_{i,t}^{rate}$ denotes the feeder load rate; $d_{i,t}$ denotes the device status mark; W_a^r and b_a^r denote the response mapping parameters. The formula transforms the estimation results into structured outputs that can be called by the system interface, so that the state estimation extends from numerical calculation to running application.

After the above processing, the model output consists of state variables, branch states, operation categories, and response vectors. The results can not only be used for online display, but also retain input slices and topology versions for subsequent review. Therefore, the state estimation results have the application properties of discriminability, callability and traceability.

3.4 Reliability verification and interpretability analysis of estimation results

When the state estimation results are used to discriminate the operation of distribution networks, it is not enough to give only the values of voltage, current or power for online applications. In the process of multi-source data fusion, there may be communication delay, terminal drift, spurious measurement error and topology version difference, so the estimation results need to be checked before entering the application layer. This check not only compares the deviation between the predicted and measured values, but also checks whether the results conform to the branch connectivity, node power balance, and historical state changes. At the same time, the model should also state which data sources, node characteristics or branch relationships are mainly affected by a certain estimation result. Based on this computational requirement, this section constructs the residual credibility score, uncertainty quantification, physical consistency check and feature contribution analysis links, so that the state estimation results have the technical attributes of reviewable, traceable and interpretable.

In order to test the consistency between the estimated results and the original measurements, a residual confidence score with source weights should be constructed, which is calculated as follows:

$$\chi_{i,t} = \exp\left(-\sum\nolimits_{k\in\mathcal{M}_i} \omega_{k,t} \frac{\|y_{k,t} - \mathcal{H}_k(x_{i,t}^c)\|_2^2}{\sigma_k^2 + \varepsilon}\right) \tag{16}$$

Here, $\chi_{i,t}$ denotes the residual credibility score; $y_{k,t}$ denotes the k original measurement; $\mathcal{H}_k$ denotes the observation function that inverts the measurement value from the estimated state; $\omega_{k,t}$ denotes the measurement source weight; Let σ_k^2 denote the noise scale; Let ε denote the stable term. This equation incorporates the residual size and source quality into the score at the same time to avoid the outlier of low-quality terminals dominating the credibility judgment.

The estimation results also need to give the uncertainty range. For the multi-source fusion model, the uncertainty comes from both the model inference fluctuation and the data source noise, so the two types of factors need to be calculated at the same time.

In order to describe the uncertainty caused by model inference fluctuation and multi-source measurement noise, it is necessary to fuse the perturbation inference variance with the source-level noise, which is calculated as follows:

$$u_{i,t} = \mathrm{Tr}\left(\frac{1}{B-1}\sum_{b=1}^{B}(x_{i,t}^{(b)} - \bar{x}_{i,t})(x_{i,t}^{(b)} - \bar{x}_{i,t})^{\top}\right) + \lambda_n \sum_{s=1}^{S}(1 - c_{s,i,t})\sigma_s^2 \quad (17)$$

where $u_{i,t}$ represents the estimation uncertainty;$x_{i,t}^{(b)}$ represents the reasoning result of the b disturbance; $\bar{x}_{i,t}$ denote the average estimate; $c_{s,i,t}$ represent the trust weight of the data source; Let σ_s^2 denote the source-level noise intensity; Let λ_n denote the noise fusion coefficient. This formula reflects both the model output fluctuation and the data quality difference, so that the confidence is no longer dependent on the single estimation error.

Physical consistency check is used to check whether the estimation results satisfy the basic operation relationship of the distribution network. If the error of a state variable is small, but the deviation from power flow balance or topology constraint is large, this result still needs to be marked.

Fig. 4 is used to illustrate the recheck link for credibility check and interpretable analysis. In the left part of the figure, the state estimation results are input, including node state, branch state and running label. The middle part is the review calculation layer, which completes the residual credibility score, uncertainty calculation, physical consistency check and contribution analysis in turn. The right side outputs the trust level, abnormal source location and key impact characteristics. At the bottom, the result library is connected with the review record to store the measurement segments, topology versions, and interpretation results.

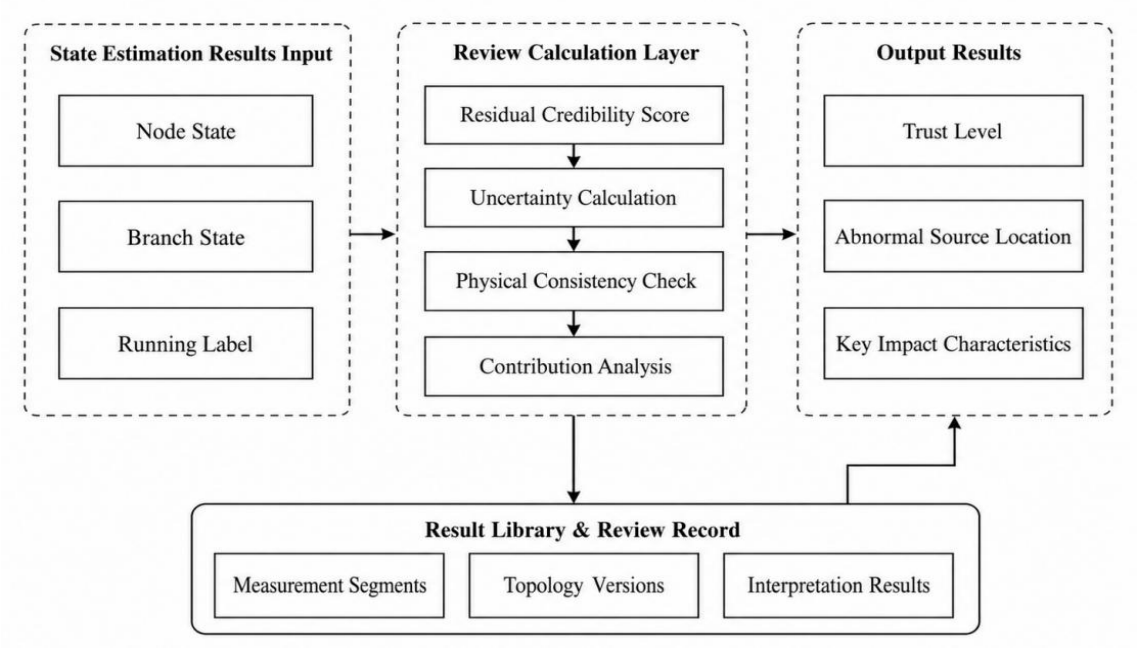

Figure 4: Estimation results credibility verification and interpretable analysis process

In order to judge whether the estimation matrix conforms to the branch connectivity and node power balance, a physical consistency check function should be constructed, which is calculated as follows:

$$\zeta_t = \frac{1}{|\mathcal{N}| + |\mathcal{E}|}\|\mathcal{F}(X_t^c, \Theta_t) - 0\|_2 + \mu\|B_t X_t^c - q_t\|_1 \quad (18)$$

Here, ζ_t denotes the physical consistency deviation; X_t^c represents the corrected state

matrix of the whole network; $\mathcal{F}(\cdot)$ represents the power flow constraint operator; Θ_t denotes the line parameters under the topology version; B_t stands for topological incidence matrix; q_t represents the node power balance term. This formula is used to find cases where the numerical estimate is inconsistent with the physical operation relationship.

Interpretable analysis needs to account for the effect of input features on specific state variables. In this paper, the disturbance contribution calculation is used to observe the output change after replacing a certain type of input with a benchmark sample, so as to locate the key source.

In order to identify the contribution of different data sources and state characteristics to the estimation results, it is necessary to establish the disturbance contribution decomposition function, which is calculated as follows:

$$\Gamma_{d,l} = \frac{1}{B}\sum_{b=1}^{B}\left[f_l(S_t^0) - f_l(S_t^0 \leftarrow d: S_{base}^{(b)})\right] \tag{19}$$

Here, $\Gamma_{d,l}$ denotes the contribution of type d input to the l state variable.$f_l(\cdot)$ denotes the l output of the state estimation function; $S_{base}^{(b)}$ denotes the b base substitution sample. This formula can correspond the contribution results to the data source, node location and state variables, and facilitate the interpretation of the main sources of voltage offset, branch overload or load surge.

The final trustworthiness level needs to fuse residual score, uncertainty, physical deviation and key contribution features. The results not only serve the system automatic screening, but also facilitate manual review.

To generate a trustworthiness level that can be written into the system result library, the residual, uncertainty, physical consistency, and interpretation contribution should be integrated, which is calculated as follows:

$$C_{i,t} = \sigma\left(\omega_1\chi_{i,t} - \omega_2 u_{i,t} - \omega_3\zeta_t + \omega_4 \mathrm{TopK}(\Gamma_{:,i}) + b_c\right) \tag{20}$$

where $C_{i,t}$ denotes the final trustworthiness level; $\chi_{i,t}$ denotes the residual confidence score; $u_{i,t}$ denotes uncertainty; Let ζ_t denote the physical consistency deviation;$\mathrm{TopK}(\Gamma_{:,i})$ is the set of key contribution features. ω_1 to ω_4 represent the fusion weights. This formula compresses the multi-class verification results into a unified trust level, and retains the basis of classification.

After the above verification, the state estimation results can present numerical value, confidence and interpretation basis at the same time. The results with high confidence can be put into operation monitoring, and the results with low confidence can retain the abnormal sources and measurement fragments. This mechanism makes the model output reviewable, and also provides a basis for subsequent sample reflux and model update.

4 Experimental Evaluation

4.1 Experimental Design

The experimental design focuses on the accuracy, stability and deployment ability of multi-source data fusion state estimation. The IEEE 33-node distribution network simulation set and the measured set of a provincial distribution network are selected for the data part. The simulation set was generated by OpenDSS, including voltage, current, active power, reactive power, switching state and load disturbance fields, forming a total of 52,800 samples. The

measured set comes from distribution automation systems, smart meters, feeder terminals, and environmental sensors from 2021 to 2024 and contains a total of 286,000 operational records. The time window of the two types of data is reconstructed according to the estimated time, and the training set, validation set and test set are divided by 7:1.5:1.5 to avoid the intersection of data in adjacent periods into the set.

The experimental comparison objects include weighted least squares, dynamic matrix completion, random forest, MLP, LSTM, GCN, GAT and the proposed model. The traditional model is used to test the physical constraints and linear estimation ability, the machine learning model is used to test the nonlinear fitting ability, and the graph model is used to test the topological embedding effect. The model in this paper uses AdamW optimizer, the initial learning rate is 0.0003, the batch size is 64, and the maximum number of training rounds is 180. The training was stopped when the validation set did not drop for 12 consecutive rounds. Time alignment, missing compensation, confidence weight calculation, and node-level normalization are uniformly performed at the input, and the topology version is saved synchronously with the samples. The specific experimental setup is shown in Table II.

Table 2: Experimental datasets and model configurations

Item	Setting	Description
Simulation dataset	IEEE 33-node system, 52,800 samples	Used to verify the estimation accuracy of the model under standard topology
Measured dataset	Provincial distribution network from 2021 to 2024, 286,000 records	Used to verify the online adaptability under multi-source heterogeneous data
Input data	SCADA, PMU, smart meters, feeder terminal units, environmental sensors	Corresponding to state features, topology mapping, and credibility verification
Comparative models	WLS, dynamic matrix completion, RF, MLP, LSTM, GCN, GAT	Covering traditional estimation, machine learning, and graph-based models
Training setting	AdamW, learning rate of 0.0003, batch size of 64, 180 epochs	Training stops when the validation loss does not decrease for 12 consecutive epochs
Evaluation metrics	Voltage MAE, phase angle RMSE, accuracy, F1, inference latency	Covering numerical estimation, state identification, and deployment efficiency

The evaluation metrics are voltage MAE, phase Angle RMSE, state recognition accuracy, F1 score and inference delay. The voltage MAE is used to measure the numerical deviation of node state, the phase Angle RMSE is used to observe the stability of phase estimation, the state recognition accuracy and F1 value are used to test the operation state discrimination results, and the inference delay is used to measure the deployment feasibility. The experimental environment uses Python 3.10 and PyTorch 2.1, the training equipment is NVIDIA RTX 4090, and the test is completed on the edge computing node. All models were run five times repeatedly, and the results were averaged with standard deviation to reduce fluctuations caused by random initialization. The design can verify the contribution of four modules: multi-source fusion, topology mapping, state discrimination and trusted verification.

4.2 Experimental Results

The experimental results are carried out from four aspects: state estimation accuracy, running state discrimination, module ablation and credibility verification. The test data includes the IEEE 33-node simulation set and the provincial distribution network measured set, and the input covers SCADA, PMUs, smart meters, feeder terminals and environmental sensors. All models were run five times repeatedly under the same data partition, and the results were averaged and evaluated by voltage MAE, phase Angle RMSE, branch current MAE, state recognition accuracy, and inference delay.

Fig. 5 is used to present the distribution of node voltage estimation errors for different models on the provincial measured set. The boxes of WLS and dynamic matrix completion are wider, which indicates that the error is greatly affected by the node position and measurement integrity. The median error of GCN and GAT decreases, but there is still a long-tail error in the end feeder. The median error of the model in this paper is close to 0.011 p.u., and the main error is concentrated in 0.008-0.017 p.u. Between, indicating that the multi-source confidence weight and neighborhood compensation mechanism can weaken the fluctuation caused by low observation nodes.

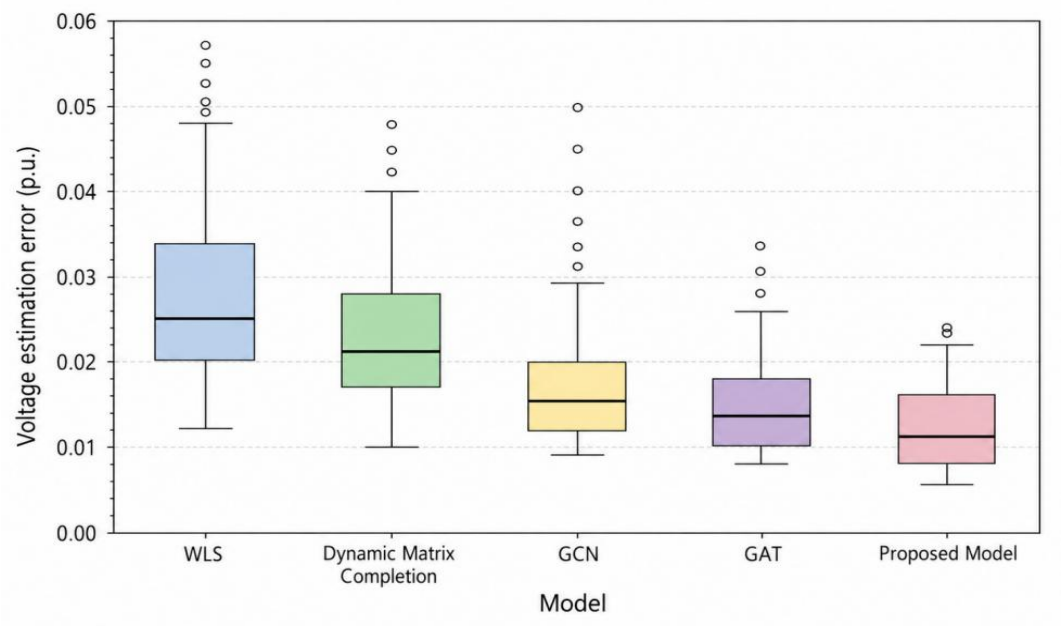

Figure 5: Box plot of node voltage estimation error

To compare the comprehensive performance of different models, Table 3 lists the test results of traditional estimation methods, machine learning models, time series models, graphical models, and the proposed model. The delay of WLS and dynamic matrix completion is lower, but the voltage MAE is 0.0318 p.u. And 0.0275 p.u., the branch current error is also higher. After introducing the topology with GCN and GAT, the voltage MAE drops to 0.0164 p.u. And 0.0152 p.u. In this paper, the model is further reduced to 0.0136 p.u., and the state recognition accuracy reaches 96.2%, which indicates that multi-source fusion and topology mapping can support the estimation accuracy and state discrimination.

Table 3: Comparison of state estimation performance of different models

Model	Voltage MAE / p.u. ↓	Phase Angle RMSE / ° ↓	Branch Current MAE / A ↓	State Identification Accuracy / % ↑	Latency / ms ↓
WLS	0.0318	1.426	18.74	84.6	6.2
Dynamic Matrix Completion	0.0275	1.218	15.39	87.9	9.5
RF	0.0241	1.064	13.82	89.3	11.8
MLP	0.0217	0.936	12.46	91.0	13.4
LSTM	0.0189	0.812	10.73	92.7	16.1
GCN	0.0164	0.734	9.18	94.1	17.3
GAT	0.0152	0.698	8.61	95.0	19.4
Proposed Model	0.0136	0.621	7.84	96.2	18.7

Fig. 6 is used to present the results of operation state discrimination, and the categories include normal operation, voltage overlimit, load surge, branch overload and abnormal measurement. The diagonal of the matrix represents the proportion of each class that is correctly identified, and the off-diagonal region is used to observe sources of confusion. The recognition rate of normal operation category is 97.4%, the recognition rate of voltage over-limit is 96.8%, and the recognition rate of branch overload is 95.6%, which indicates that the state estimation results can well support the output of operation state. There is still a small amount of confusion between the abnormal measurement and the sudden load increase, the main reason is that the delayed upload of smart meters and the rapid change of station load overlap in the time window. The model needs to rely on the credibility verification layer to further distinguish between "real state change" and "data source anomaly".

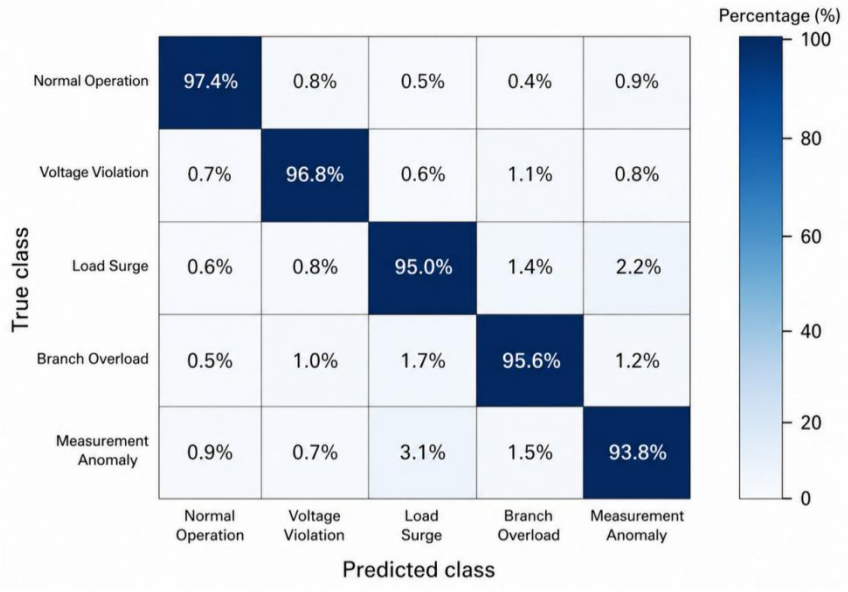

Figure 6: Confusion matrix diagram for running state discrimination

Table 4 is used to analyze the contribution of modules inside the model. After removing the topology embedding, the voltage MAE increases to 0.0196 p.u. and the phase Angle RMSE increases to 0.846°, which indicates that the connection relationship between nodes and branches has a direct constraint effect on the state estimation. After removing the multi-source confidence weights, the F1-score was reduced to 0.921, indicating that the model

was difficult to distinguish between highly reliable PMU segments and delayed smart meter data. After removing the residual gating, the disturbance of the abnormal measurement on the estimation results is enhanced. After removing the trusted verification, the voltage MAE does not change much, but the credibility agreement rate drops to 86.5%, indicating that the module mainly assumes the function of result review and abnormal source identification. The full model remains optimal on the four indicators, which indicates that there is a complementary relationship between the modules.

Table 4: Results of model ablation experiments

Model Setting	Voltage MAE / p.u. ↓	Phase Angle RMSE / ° ↓	F1-score ↑	Credibility Consistency / % ↑
Without Multi-source Confidence Weighting	0.0179	0.792	0.921	90.8
Without Topology Embedding	0.0196	0.846	0.907	89.4
Without Residual Gating	0.0168	0.751	0.933	91.7
Without Credibility Verification	0.0159	0.713	0.941	86.5
Complete Model	0.0136	0.621	0.958	95.3

Fig. 7 is used to show the spatial distribution of estimation errors at different feeder nodes. The errors of the core feeder F2 and F4 are mainly concentrated in 0.010-0.014 p.u., which indicates that the estimation results of the dense measurement area are more stable. The local node error of the end feeder F7 is about 0.018 p.u., but there is no continuous diffusion phenomenon, which indicates that topological embedding and neighborhood aggregation form a complement to the end low observation nodes.

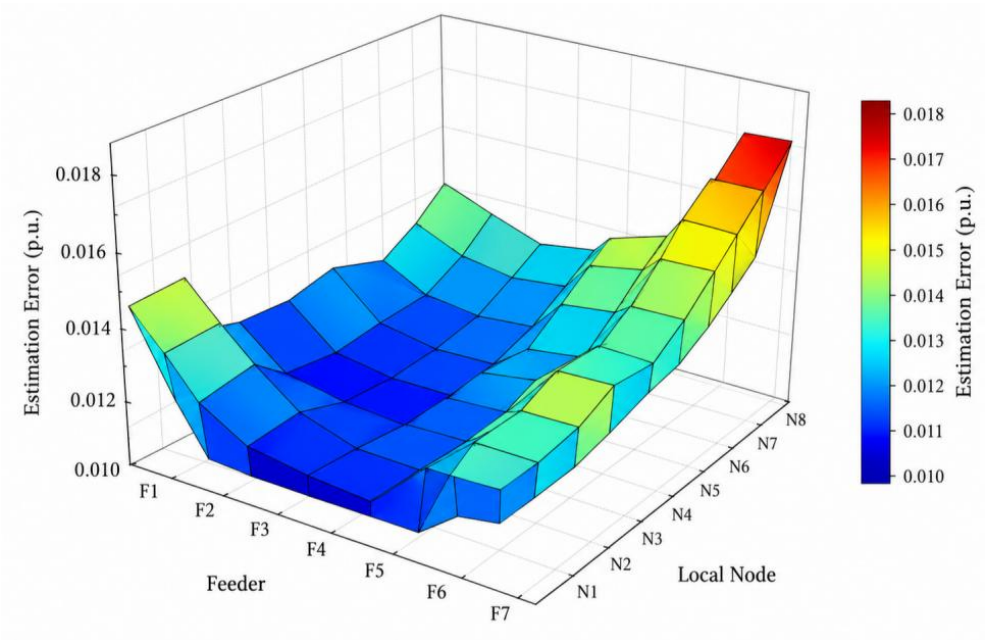

Figure 7: Thermodynamic matrix plot of estimation error at feeder nodes

Table 5 is used to show the correspondence between the credibility level and the estimation error, focusing on checking whether the credibility check module has the actual

discrimination ability. The proportion of high-confidence samples was 71.6%, the voltage MAE was 0.0109 p.u., and the abnormal source location rate reached 97.1%. The proportion of credible samples was 22.8%, and the voltage MAE was 0.0158 p.u.; The low-confidence samples accounted for 5.6%, the voltage MAE increased to 0.0237 p.u., and the average delay also increased to 20.4 ms. The low-confidence samples are mainly concentrated in the segments of communication delay, high proportion of missing compensation and topology version switching. The result shows that the trust level is not a formal label, but can reflect the real difference between estimation error, anomaly localization ability and computational overhead.

Table 5: Correspondence between credibility level and estimation error

Credibility Level	Sample Proportion / %	Voltage MAE / p.u. ↓	Abnormal Source Localization Rate / % ↑	Average Latency / ms
High Credibility	71.6	0.0109	97.1	17.9
Medium Credibility	22.8	0.0158	93.4	18.6
Low Credibility	5.6	0.0237	88.2	20.4

Fig. 8 is used to show the comprehensive performance of the model under multi-dimensional indicators. The normalized scores of the five items of the model in this paper are 0.962, 0.958, 0.953, 0.941 and 0.936, respectively, and the overall contour is closer to the outer circle, indicating that the model maintains a relatively balanced performance among state estimation, operation discrimination, credible review and online execution. GCN and GAT have advantages in topology modeling, but the credibility agreement rate and abnormal source location rate are lower than the proposed model, which indicates that simple graph structure learning is still not enough to cover the review requirements under multi-source heterogeneous data.

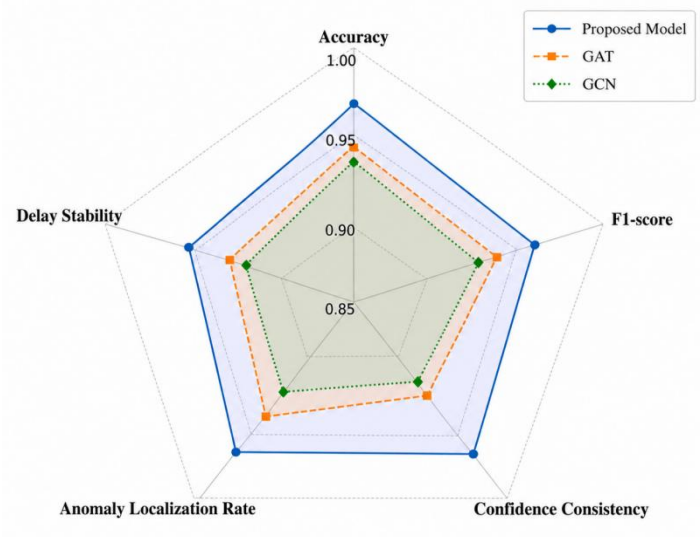

Figure 8: Radar chart of comprehensive performance of the state estimation model

Combined with the above results, multi-source data fusion improves the stability of asynchronous measurement input, topology embedding reduces the branch correlation error, residual gating weakens the disturbance of local abnormal measurements, and confidence checking enhances the ability to review the estimation results. The proposed model achieves

0.0136 p.u. voltage MAE, 96.2% state recognition accuracy and 18.7 ms average inference delay on provincial measured data, which can support online state estimation applications of smart distribution networks.

5 Discussion

The results of the proposed model on the IEEE 33-node simulation set and the provincial measured data show that the performance gain of multi-source fusion state estimation comes from the synergy of data layer, topology layer and review layer. Compared with WLS and dynamic matrix completion, the model no longer relies on fixed weights and static pseudo-measurements, but uses SCADA, PMU, smart meter, feeder terminal and environmental sensors to form a unified feature, so that the voltage MAE is reduced to 0.0136 p.u. Compared with LSTM, GCN and GAT, the model not only extracts temporal variation and node association, but also puts measurement confidence, branch embedding and residual gating into the same computing link. Ablation results show that the voltage MAE rises to 0.0196 p.u. after removing the topological embedding, which indicates that the branch relationship has a direct constraint on the estimation results. After removing the trusted verification, the consistency rate decreases to 86.5%, which indicates that the review layer is mainly responsible for locating the source of anomalies and judging the availability of results. Figs. 5 to 8 further illustrate that the model maintains relatively stable performance in low observation end nodes, running state discrimination and comprehensive indicators, which is suitable for online estimation scenarios. This result indicates that the value of the fusion strategy is not a single error reduction, but rather that the estimates, state labels, and double-check evidence are kept as a complete record of the same origin.

6 Conclusions

Focusing on the task of multi-source data fusion state estimation in smart distribution grid, this paper constructs a computational framework consisting of data fusion, topology embedding, state discrimination and trusted verification. The model maps SCADA, PMU, smart meter, feeder terminals and environmental sensor records into the state feature space, and uses the graph structure to express the operation association between nodes, branches, switches and transformers. Experimental analysis shows that the proposed framework can maintain stable estimation output under the conditions of asynchronous sampling, missing measurements and topology changes, and provide a recheck basis for the identification of voltage overruns, load spikes, branch overloads and measurement anomalies. The limitations of this paper are reflected in the fact that the data sources are concentrated in a limited area, and the extreme weather, complex switching and high proportion of distributed power access scenarios are insufficient coverage. Edge-side deployment focuses on reasoning and verification, and the model update mechanism in a continuous operation environment has not yet been formed. In the future, the scalable cross-regional samples are studied, and the federated learning, lightweight graph network and incremental learning methods are combined to enhance the adaptability of the model under the conditions of multi-site data isolation, frequent topology changes and terminal computing power limitation. At the same time, the credibility verification results can be linked with the alarm rules of the master station and the digital twin simulation to form a sample reflux and model iteration link, which makes the state estimation results more suitable for end-online operation.

References

[1] Rout B, Dahale S, Natarajan B. Dynamic matrix completion based state estimation in distribution grids[J]. IEEE Transactions on Industrial Informatics, 2022, 18(11): 7504-7511.

[2] Raghuvamsi Y, Teeparthi K. Detection and reconstruction of measurements against false data injection and DoS attacks in distribution system state estimation: A deep learning approach[J]. Measurement, 2023, 210: 112565.

[3] Asefi S, Mitrovic M, Ćetenović D, et al. Anomaly detection and classification in power system state estimation: Combining model-based and data-driven methods[J]. Sustainable Energy, Grids and Networks, 2023, 35: 101116.

[4] Ganjkhani M, Abbaspour A, Fattaheian-Dehkordi S, et al. Application of machine learning in determining and resolving state estimation anomalies in power systems[J]. Sustainable Energy, Grids and Networks, 2024, 38: 101335.

[5] Kundacina O, Cosovic M, Miskovic D, et al. Graph neural networks on factor graphs for robust, fast, and scalable linear state estimation with PMUs[J]. Sustainable Energy, Grids and Networks, 2023, 34: 101056.

[6] Habib B, Isufi E, van Breda W, et al. Deep statistical solver for distribution system state estimation[J]. IEEE Transactions on Power Systems, 2023, 39(2): 4039-4050.

[7] Dabush L, Kroizer A, Routtenberg T. State estimation in partially observable power systems via graph signal processing tools[J]. Sensors, 2023, 23(3): 1387.

[8] Cooper A, Bretas A, Meyn S. Anomaly detection in power system state estimation: Review and new directions[J]. Energies, 2023, 16(18): 6678.

[9] Vijaychandra J, Prasad B R V, Darapureddi V K, et al. A review of distribution system state estimation methods and their applications in power systems[J]. Electronics, 2023, 12(3): 603.

[10] Békési G, Barancsuk L, Hartmann B. Deep neural network based distribution system state estimation using hyperparameter optimization[J]. Results in Engineering, 2024, 24: 102908.

[11] Táczi I, Vokony I, Barancsuk L, et al. Role of voltage control devices in low voltage state estimation process[J]. International Transactions on Electrical Energy Systems, 2023, 2023(1): 6614905.

[12] Barancsuk L, Hartmann B. Analysis of state estimation accuracy in distribution networks using pseudo-measurement selection and real measurement incorporation[J]. 2024.

[13] Nguyen B L H, Vu T V, Nguyen T T, et al. Spatial-temporal recurrent graph neural networks for fault diagnostics in power distribution systems[J]. IEEE Access, 2023, 11: 46039-46050.

[14] Alhanaf A S, Balik H H, Farsadi M. Intelligent fault detection and classification schemes for smart grids based on deep neural networks[J]. Energies, 2023, 16(22): 7680.

[15] Tabassum T, Toker O, Khalghani M R. Cyber–physical anomaly detection for inverter-based microgrid using autoencoder neural network[J]. Applied Energy, 2024, 355: 122283.

[16] Mirzaee P H, Shojafar M, Cruickshank H, et al. Smart grid security and privacy: From conventional to machine learning issues (threats and countermeasures)[J]. IEEE access, 2022, 10: 52922-52954.

[17] Biswal B, Deb S, Datta S, et al. Review on smart grid load forecasting for smart energy management using machine learning and deep learning techniques[J]. Energy Reports, 2024, 12: 3654-3670.

[18] Massignan J A D, London J B A, Bessani M, et al. Bayesian inference approach for information fusion in distribution system state estimation[J]. IEEE Transactions on Smart Grid, 2021, 13(1): 526-540.

[19] Da Silva L P Q, de Souza J C S, Do Coutto Filho M B. Generative neural networks for providing pseudo-measurements in electric power distribution systems[J]. Journal of the Brazilian Computer Society, 2024, 30(1): 155-162.

[20] Radhoush S, Vannoy T, Liyanage K, et al. Distribution system state estimation and false data injection attack detection with a multi-output deep neural network[J]. Energies, 2023, 16(5): 2288.

[21] Buchta E, Duckheim M, Metzger M, et al. Leveraging behavioral correlation in distribution system state estimation for the recognition of critical system states[J]. Energies, 2023, 16(20): 7180.